Assembly of the Eukaryotic PLP-Synthase Complex from *Plasmodium* and Activation of the Pdx1 Enzyme

Gabriela Guédez,[1] Katharina Hipp,[2] Volker Windeisen,[1] Bianca Derrer,[3,4] Martin Gengenbacher,[3,5] Bettina Böttcher,[2] Irmgard Sinning,[1] Barbara Kappes,[3] and Ivo Tews[1,6,*]

[1]Heidelberg University Biochemistry Center (BZH), Im Neuenheimer Feld 328, 69120 Heidelberg, Germany
[2]The University of Edinburgh, School of Biological Sciences, Institute of Structural & Molecular Biology, King's Buildings, Mayfield Road, Edinburgh EH9 3JR, UK
[3]Department of Infectious Diseases, Parasitology, University Hospital Heidelberg, Im Neuenheimer Feld 324, 69120 Heidelberg, Germany
[4]Present address: Institute of Medical Biotechnology, Paul-Gordan-Str. 3, 91052 Erlangen, Germany
[5]Present address: Department of Immunology, Max-Planck-Institute for Infection Biology, Charitéplatz 1, 10117 Berlin, Germany
[6]Present address: University of Southampton, Centre for Biological Sciences, Institute for Life Sciences (IfLS), Southampton SO17 1BJ, UK
*Correspondence: ivo_tews@yahoo.com
DOI 10.1016/j.str.2011.11.015

SUMMARY

Biosynthesis of vitamins is fundamental to malaria parasites. Plasmodia synthesize the active form of vitamin B_6 (pyridoxal 5′-phosphate, PLP) using a PLP synthase complex. The EM analysis shown here reveals a random association pattern of up to 12 Pdx2 glutaminase subunits to the dodecameric Pdx1 core complex. Interestingly, *Plasmodium falciparum* PLP synthase organizes in fibers. The crystal structure shows differences in complex formation to bacterial orthologs as interface variations. Alternative positioning of an α helix distinguishes an open conformation from a closed state when the enzyme binds substrate. The pentose substrate is covalently attached through its C1 and forms a Schiff base with Lys84. Ammonia transfer between Pdx2 glutaminase and Pdx1 active sites is regulated by a transient tunnel. The mutagenesis analysis allows defining the requirement for conservation of critical methionines, whereas there is also plasticity in ammonia tunnel construction as seen from comparison across different species.

INTRODUCTION

Plasmodium falciparum (*Pf*), *Plasmodium vivax*, *Plasmodium malariae*, *Plasmodium ovale*, and *Plasmodium knowlesi* are human pathogens of the malaria disease. Malaria is a serious threat to human health with nearly 250 million cases worldwide, and about 1 million deaths annually (World Health Organization, 2010). Despite significant advances in the understanding of the disease as well as the parasite's biology and metabolism (Lakshmanan et al., 2011), malaria is still one of the leading causes of morbidity and mortality in developing countries, especially in sub-Saharan Africa, but also in Asia and Latin America (World Health Organization, 2010). A major factor hindering malaria control is the high degree of resistance developed by

Plasmodium species against currently available drugs (Bustamante et al., 2009; Petersen et al., 2011; Travassos and Laufer, 2009). Hence, there is still an urgent need for the identification of novel drug targets as well as antimalarial chemotherapeutics (Burrows et al., 2011; Kappes et al., 2011).

Although plasmodia rely on host-derived nutrients (Divo et al., 1985), certain essential cofactors need to be produced by the parasite. Vitamin biosynthetic pathways in general (Müller et al., 2010; Müller and Kappes, 2007; Wrenger et al., 2008) and vitamin B_6 biosynthesis in particular (Gengenbacher et al., 2006; Wrenger et al., 2005) have attracted interest as potential drug targets. Although humans depend on vitamin uptake, plasmodia possess a de novo pathway for vitamin B_6 biosynthesis, constituted by the *pdx1* and *pdx2* genes. *Pf* expresses functional orthologs of the *pdx1* and *pdx2* genes in blood stages (Gengenbacher et al., 2006; Wrenger et al., 2005), a prerequisite for an antimalarial drug target. Furthermore, the expression in intra-erythrocytic stages suggests that de novo vitamin B_6 biosynthesis is vital for parasite development. Other pathogenic organisms that express the *pdx1* and *pdx2* genes are *Toxoplasma* (Knöckel et al., 2007) and *Mycobacterium* (Dick et al., 2010).

Pyridoxal 5′-phosphate, PLP, an active form of vitamin B_6, is a widely used enzymatic cofactor in enzymes involved in amino acid metabolism (Eliot and Kirsch, 2004; Percudani and Peracchi, 2003); PLP has also an important role as an antioxidant (Ehrenshaft et al., 1999; Mooney and Hellmann, 2010). This function may indeed be required for intracellular survival within red blood cells, a developmental phase concurrent with marked oxidative stress (Müller, 2004; Wrenger et al., 2005).

De novo PLP biosynthesis by Pdx1 requires the substrates ribose 5-phosphate (R5P) and glyceraldehyde 3-phosphate (G3P) (Burns et al., 2005; Fitzpatrick et al., 2007; Raschle et al., 2005). The heterocyclic nitrogen is derived through hydrolysis of L-glutamine by Pdx2 (Tanaka et al., 2000; Tazuya et al., 1995). The two enzymes form the PLP synthase complex, functionally classified as a glutamine amidotransferase (Zalkin and Smith, 1998). PLP synthase assembles a total of 12 Pdx1 PLP synthase subunits (Neuwirth et al., 2009; Strohmeier et al., 2006; Zhu et al., 2005) and up to 12 Pdx2 glutaminase subunits (Strohmeier et al., 2006; Zein et al., 2006; Figure 1). The architecture of the complex is known from 3D structures
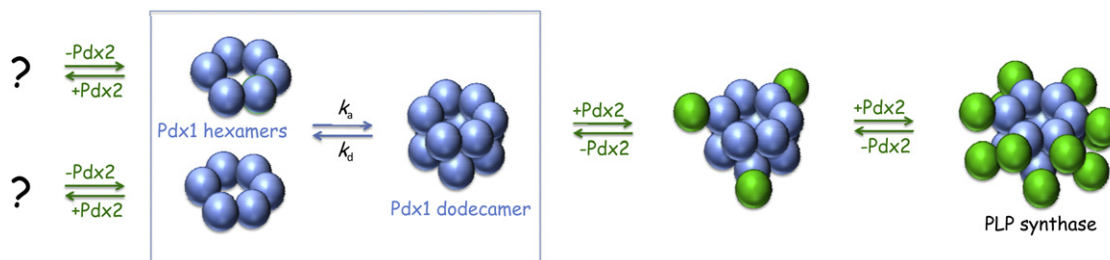
Figure 1. Assembly of PLP Synthase from Pdx1 and Pdx2 Proteins
The synthase subunit, Pdx1, is in hexamer-dodecamer equilibrium (Strohmeier et al., 2006; Zhu et al., 2005). When glutaminase Pdx2 is added, it is assumed to independently bind to Pdx1 subunits, until the saturated complex of 24 subunits is formed (Müller et al., 2008; Neuwirth et al., 2007; Strohmeier et al., 2006). To our knowledge, whether Pdx2 forms complexes with Pdx1 hexamers is unknown.

of bacterial enzymes, but to our knowledge, no structure of a eukaryotic Pdx1/Pdx2 PLP synthase complex is available to date.

Prokaryotic Pdx1 proteins had previously shown to be mainly dodecameric (Strohmeier et al., 2006; Zhu et al., 2005). In contrast, Pdx1 from the yeast *Saccharomyces cerevisiae* has been characterized structurally, and it differs from prokaryotic and eukaryotic orthologs by a small insertion responsible for a shift in hexamer-dodecamer equilibrium toward the hexameric form (Neuwirth et al., 2009). Hence, it was speculated that prokaryotic and eukaryotic enzymes have a different mode of regulation.

Biochemical and biophysical characterizations of *Pf* PLP synthases revealed further differences (Flicker et al., 2007). It was noted that the complexes of eukaryotic and prokaryotic systems have different thermodynamic signatures in isothermal titration calorimetry (Flicker et al., 2007; Neuwirth et al., 2007). This is surprising because activation of Pdx2 by interaction with Pdx1 was thought to be similar in all systems. It was shown that these differences are more pronounced in the absence of the substrate L-glutamine and vanished in the presence of substrate in the activated Michaelis complex (Flicker et al., 2007). The 3D structural analysis of plasmodial PLP synthase complex described here explains these differences in the Pdx1/Pdx2 interaction. We also studied a substrate complex and provide biochemical evidence for how the $(\beta/\alpha)_8$ barrel of Pdx1 functions in ammonia transfer. The data provide a better understanding of enzyme regulation and highlight features and differences in eukaryotic and prokaryotic PLP synthases that may be exploitable in future drug design.

RESULTS

Fiber Formation of Recombinant PLP Synthase from *Plasmodium falciparum*
In order to structurally characterize the malarial PLP synthase, Pdx1 and Pdx2 from *Pf* were recombinantly expressed and purified to homogeneity. Our dynamic light scattering confirmed that both proteins were monodisperse and suited for crystallization (data not shown). *Pf*Pdx1 and *Pf*Pdx2 proteins were reconstituted into the PLP synthase complexes. Crystallization trials were set up in the absence or presence of substrate L-glutamine. Instead of using the native *Pf*Pdx2 enzyme, we employed a *Pf*Pdx2[H196N] catalytically inactive variant to avoid hydrolysis of the substrate. Exchange of the catalytic triad histidine with

asparagine allows formation of a stable PLP synthase complex in the presence of substrate (Flicker et al., 2007; Neuwirth et al., 2007; Strohmeier et al., 2006). Despite all efforts, no suitable crystals for X-ray diffraction analysis were obtained.

To understand what interfered with crystal formation, the *Pf* proteins were further analyzed by electron microscopy (EM) and single-particle image processing. The analysis showed that the autonomous *Pf*Pdx1 subunit formed cylinders (Figure 2A), which matched the dodecameric complex in shape and size observed in crystal structures of bacterial complexes (Strohmeier et al., 2006; Zein et al., 2006; see model of the PLP synthase assembly in Figure 1). Furthermore, dynamic light-scattering experiments and size-exclusion chromatography independently confirmed this dodecameric species (see Figure S1A available online).

Surprisingly, PLP synthase complexes reconstituted from *Pf*Pdx1 and *Pf*Pdx2 formed fibers (Figure 2B). Comparing the spacing between the layers in the fibers (Figure 2B, inset) with the *B. subtilis* (*Bs*) crystal structure of *Bs*Pdx1/*Bs*Pdx2 (Strohmeier et al., 2006) suggested that the fibers consisted of stacked 24-mer with the longer distance between layers in the fibers being internal to the 24-mer. To address whether fiber formation is a specific property of the *Pf* PLP synthase, we studied PLP synthase complexes from the bacterium *Bs* and from the mouse malaria parasite *P. berghei* (*Pb*). In a similar EM analysis, we used the inactivated *Bs*Pdx2[H170N] (Neuwirth et al., 2007; Strohmeier et al., 2006) and *Pb*Pdx2[H199N] (constructed in analogy to the *Pf*Pdx2[H196N] variant). Fiber formation was only observed when *Pf*Pdx1 was present in the sample, and this fact may explain our failure to obtain suitable crystals for *Pf* PLP synthase, whereas the *Bs* PLP synthase (Strohmeier et al., 2006) and the *Pb* PLP synthase (see below) were successfully crystallized. The finding illustrates the potential of EM when working with samples that are difficult to crystallize, in this case revealing high-order assemblies of macromolecular complexes. Although we clearly observed aggregation of protein over time (Figure S1), we had not suspected that this was an ordered process, and fiber formation would have gone unnoticed had we not wanted to study complex assembly by EM.

Fortuitous Assembly of Pdx2 Subunits to the Dodecameric Pdx1 Core Particle
The assembly of PLP synthase was investigated by electron microscopic analysis of negatively stained native proteins from
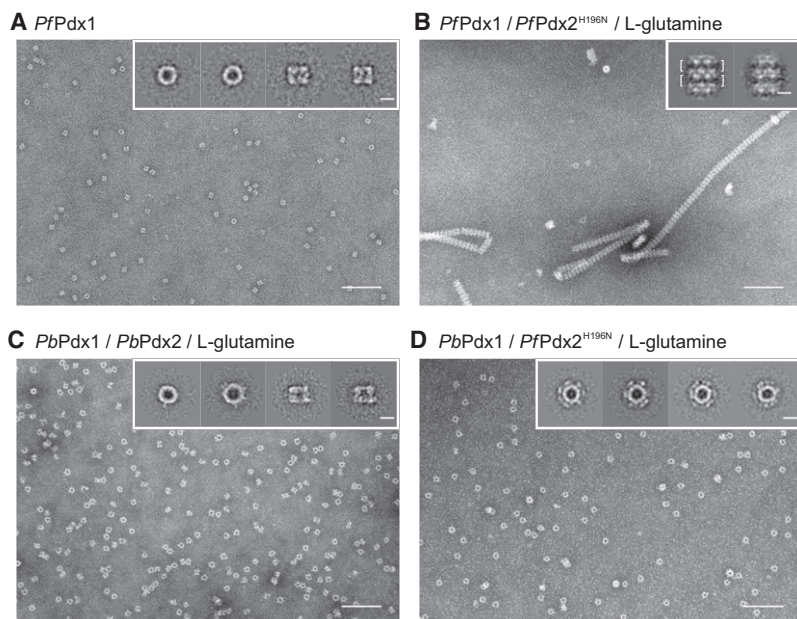
A *Pf*Pdx1

B *Pf*Pdx1 / *Pf*Pdx2[H196N] / L-glutamine

C *Pb*Pdx1 / *Pb*Pdx2 / L-glutamine

D *Pb*Pdx1 / *Pf*Pdx2[H196N] / L-glutamine

Figure 2. Electron Micrographs of Negatively Stained Plasmodial PLP Synthases

Micrographs as well as representative class averages (insets at the upper-right corners) are shown for the different complexes. The scale bars represent 100 and 10 nm on micrographs and in class averages, respectively.

(A) *Pf*Pdx1 forms dodecameric particles (compare Figure S1A).

(B) *Pf*Pdx1 in complex with *Pf*dx2[H196N] and L-glutamine forms fibers of varying length (compare Figure S1B). The class average shows two PLP synthase complexes as indicated by the lines in the inset.

(C) Variation of the occupancy of *Pb*Pdx1 dodecameric core particles with *Pb*Pdx2 in the presence of glutamine; fully occupied Pdx1 dodecamers with 12 Pdx2 protomers are not (rarely) observed.

(D) The chimeric complex used for crystallization in this study. Class averages of *Pb*Pdx1/*Pf*Pdx2[H196N]/L-glutamine show a high occupancy of *Pb*Pdx1 dodecamers with *Pf*Pdx2 subunits. Side views of the complex are almost absent in this sample.

Pb in the presence of L-glutamine because the *Pf* proteins were inaccessible to this analysis due to their tendency to form fibers. When a 1:1 stoichiometric mixture of *Pb*Pdx1 and *Pb*Pdx2 was used, multiple oligomeric species were observed (Figure 2C, compare Figure 1). Generally, *Pb*Pdx1 was seen as dodecameric core complex, but the occupancy with *Pb*Pdx2 subunits varied without discernable pattern in the distribution of *Pb*Pdx2 subunits on the *Pb*Pdx1 core, suggesting that attachment of Pdx2 is at random and, thus, most likely not cooperative. This is an important finding considering that the reaction catalyzed by Pdx1 is cooperative (Knöckel et al., 2009; Raschle et al., 2007).

Pdx1 dodecamers that were fully occupied with 12 *Pb*Pdx2 subunits were rarely observed, consistent with the behavior of the bacterial complexes in analytical ultracentrifugation (Strohmeier et al., 2006; Zhu et al., 2005). In an attempt to generate a uniform population of fully occupied complexes, a 1:1 stoichiometric mixture of *Pb*Pdx1 and *Pb*Pdx2[H199N] variant proteins was analyzed in the presence of the substrate L-glutamine. Class averages showed highly occupied as well as fully occupied complexes (data not shown). Thus, the inactivation of the Pdx2 subunit and the addition of the substrate L-glutamine increased the stability of the plasmodial PLP synthase complexes, as noted previously with bacterial samples (Strohmeier et al., 2006).

We were able to crystallize the *Pb* PLP-synthase complex, using the *Pb*Pdx1 and *Pb*Pdx2[H199N] proteins in the presence of substrate L-glutamine. Needle-shaped crystals were obtained that diffracted anisotropically to 4 and 5.5 Å at the ESRF microfocus beamline ID23-2. Data analysis suggested a low-symmetry space group with pseudo-merohedral twinning, which complicated data collection and structure determination. Because no significant improvement in crystal growth was made, structure determination was not further pursued.

However, we discovered that a complex from *Pb* Pdx1 and *Pf* Pdx2 subunits formed readily in the presence of glutamine. PLP synthase complexes with *Pb*Pdx1 dodecamers highly

occupied with *Pf*Pdx2[H196N] subunits were formed in vitro (Figure 2D). Complex formation is probably helped by the high sequence conservation: *Pf* and *Pb* Pdx1 and Pdx2 proteins are 84.5% and 63.8% identical, respectively (compare alignments in Figure S2). To test whether the chimeric complexes represented a viable model for an active PLP synthase complex, it was essential to determine enzymatic activities. Both chimeric combinations of *Pf* and *Pb* proteins were tested and compared with single-species complexes (Table 1). Complexes that contained *Pb*Pdx1 showed slightly higher PLP synthase activities than complexes that contained *Pf*Pdx1. The PLP synthase activity was not affected by the choice of the Pdx2 subunit. Similarly, when the Pdx2 glutaminase activity was assayed, we found slightly higher activities when *Pf*Pdx2 was present, regardless of the source organism for the Pdx1 subunit in the complex. Both, *Pf*Pdx2 or *Pb*Pdx2 were inactive in the absence of the respective Pdx1 subunit (Gengenbacher et al., 2006). The summarized data in Table 1 show that plasmodial chimeric complexes form catalytically competent PLP synthase species and that the Pdx1 and Pdx2 proteins within these complexes behave as in native complexes. We, therefore, carried out crystallization experiments with chimeric complexes, a strategy often employed when combining proteins from different species in structure determination of macromolecular complexes, e.g., as in the structure of *Pf* Falcipain-2 with *Pb* cysteine protease inhibitor ICP-C (Hansen et al., 2011) or the structure of the G$_{s\alpha}$-adenylyl cyclase complex, which is a rat/dog/cow chimera (Tesmer et al., 1997).

Critical Differences between Plasmodium and Bacterial PLP Synthase Complexes

Although *Pf* PLP synthase complexes formed fibers, and crystals of the *Pb* PLP synthase were of insufficient quality, we were able to grow crystals of a chimeric PLP synthase complex made up from *Pb*Pdx1 and *Pf*Pdx2[H196N] in the presence of L-glutamine. Crystals grew in a hexagonal space group, and complete data

Table 1. PLP Synthesis and Glutaminase Activities of *Pf* and *Pb* Complexes

	PLP Synthesis (nmol*min^{-1} mg^{-1})	Glutaminase Activity (nmol*min^{-1} mg^{-1})
*Pb*Pdx1/*Pb*Pdx2	1.1 ± 0.2	150 ± 12
*Pb*Pdx1/*Pf*Pdx2	1.3 ± 0.1	233 ± 14
*Pf*Pdx1/*Pf*Pdx2	0.7 ± 0.1	260 ± 28
*Pf*Pdx1/*Pb*Pdx2	0.9 ± 0.1	175 ± 20

PLP synthase-specific activity was monitored at 37°C using 40 μM Pdx1, ±40 μM Pdx2, and saturating substrate concentrations: 1 mM R5P, 1 mM G3P ± 10 mM NH$_4$Cl.

Table 2. Crystallographic Analysis

	*Pb*Pdx1	*Pb*Pdx1-R5P	*Pb*Pdx1/ *Pf*Pdx2^{H196N}/Gln
Space group	R32	R32	P6$_1$22
Cell dimensions			
a, b, c (Å)	180, 180, 102	181, 181, 102	160, 160, 583
α, β, γ (°)	90, 90, 120	90, 90, 120	90, 90, 120
Resolution (Å)	50–2.42	50–2.44	50–3.60
R$_{merge}$ (HR bin)[a]	3.6 (44.6)	4.2 (44.0)	10.6 (37.6)
I/σI (HR bin)[b]	48.7 (3.2)	46 (2.3)	10 (2)
Completeness (% HR bin)	100 (98.5)	99.9 (99.4)	96.7 (83.0)
No. of reflections	23,093	22,508	47,666
Redundancy	6.7	6.1	5.1
No. of proteins in asymmetric unit	2	2	12
Solvent content (%)	49	49	54
Refinement			
R$_{work}$[c]/R$_{free}$[d]	18.3/23.2	19.3/25.8	29.8/31.5
No. of protein atoms	4,062	4,215	23,130
No. of phosphate ion atoms	20	10	–
No. of waters	107	162	–
Ramachandran most favored (%)	93.2	92.2	84.3
Ramachandran additional allowed (%)	6.6	7.6	10.7
Ramachandran generously allowed (%)	0.2	0.2	2.5
Ramachandran disallowed (%)	0	0.0	2.5
Rmsd bond lengths (Å)	0.018	0.015	0.010
Rmsd bond angles (°)	1.678	1.507	1.293

[a] R$_{merge}$ is Σ$_j$|I$_j$−<I>|, where I$_j$ is the intensity of an individual reflection, and <I> is the average intensity for multiple recorded reflections.
[b] I/σI is the mean intensity divided by the mean error.
[c] R$_{work}$ is Σ||F$_o$|−|F$_c$||/Σ|F$_o$|, where F$_o$ is an observed amplitude, and F$_c$ is a calculated amplitude.
[d] R$_{free}$ has the same equation as R$_{work}$ and was calculated over 5% of the data that were not used for refinement.

to a resolution of 3.6 Å were collected (Table 2). Structure determination by molecular replacement was facilitated by the availability of the high-resolution models of *Pb*Pdx1, determined in this study at 2.4 Å resolution (see below), and of *Pf*Pdx2, determined earlier at 1.62 Å (Gengenbacher et al., 2006) (PDB code 2ABW).

As in the EM analysis, the PLP synthase complex contains a dodecameric Pdx1 core occupied with 12 Pdx2 subunits (Figure 2D). Superposition of the *Plasmodium* PLP synthase complex with the *Bs* complex (Strohmeier et al., 2006) showed that the Pdx2 subunit is rotated by 8.5° and displaced by 1.5 Å (Figure 3A). This analysis is based on superposition of 261 Cα positions of a single Pdx1 subunit from the 2 complexes resulting in a root-mean-square deviation (rmsd) of 0.93 Å, using lsqkab (Collaborative Computational Project, Number 4, 1994).

A good quality electron density map resulted after rigid body refinement (Figures 3B and 3C), and a number of protein segments were seen in different conformations from the input models. We carried out model building in sharpened electron density maps, followed by Translation Library Screw-motion (TLS) refinement using Non-Crystallographic Symmetry (NCS) averaging (see Experimental Procedures). Comparison with the *Bacillus* complex (Strohmeier et al., 2006) (PDB code 2NV2) aided in the building of the critical stabilizing catalytic center loop and oxyanion hole loop regions in Pdx2, residues 10–14 and 52–54 (Figure 3C), as well as in the building of Pdx1 helix α2′ (Figure 3B), residues 52–58. In addition to these regions, few segments at the interface or at the surface of the proteins were rebuilt, and these were in Pdx1, the N-terminal residues 3–9 (Figure 3B); in Pdx2, loops 95-111, 124-127, and 140-146 (Figure 3C); as well as the side chains of Arg121 and Arg154, two residues shown previously to be important for the organization of the Pdx1-Pdx2 interface (Wallner et al., 2009).

In *Bs* (Strohmeier et al., 2006) and *Thermotoga maritima* (Zein et al., 2006) PLP synthase complexes (PDB codes 2NV2 and 2ISS), helix αN of the Pdx1 subunit is essential for complex formation with and activation of the Pdx2 glutaminase subunit (Strohmeier et al., 2006; Wallner et al., 2009; Zein et al., 2006). In the two bacterial structures, the β strand βN preceding helix αN interacts with the central β sheet of Pdx2 by a mechanism called β completion (see Figure 3B). Our earlier deletion analysis indicated that in *Pf* Pdx1 the region that forms βN in bacterial complexes is not involved in interaction between Pdx1 and Pdx2 (Flicker et al., 2007). Indeed, β completion does not occur in plasmodial PLP synthase. The electron density map in this region suggests that the very N terminus is oriented toward Pdx1 and does not contact Pdx2 (Figure 3B).

The electron density map for the plasmodial PLP synthase complex resolves the loop region 124-127 that was disordered in the 1.62 Å structure of autonomous *Pf*Pdx2 (Gengenbacher et al., 2006) (PDB code 2ABW). This loop is at the interface to the Pdx1 protein, and superposes well with the equivalent regions in bacterial complexes (Figure 3C) *Pf*Pdx2 has a seven amino acid insertion between β5 and β6 (ten amino acids in
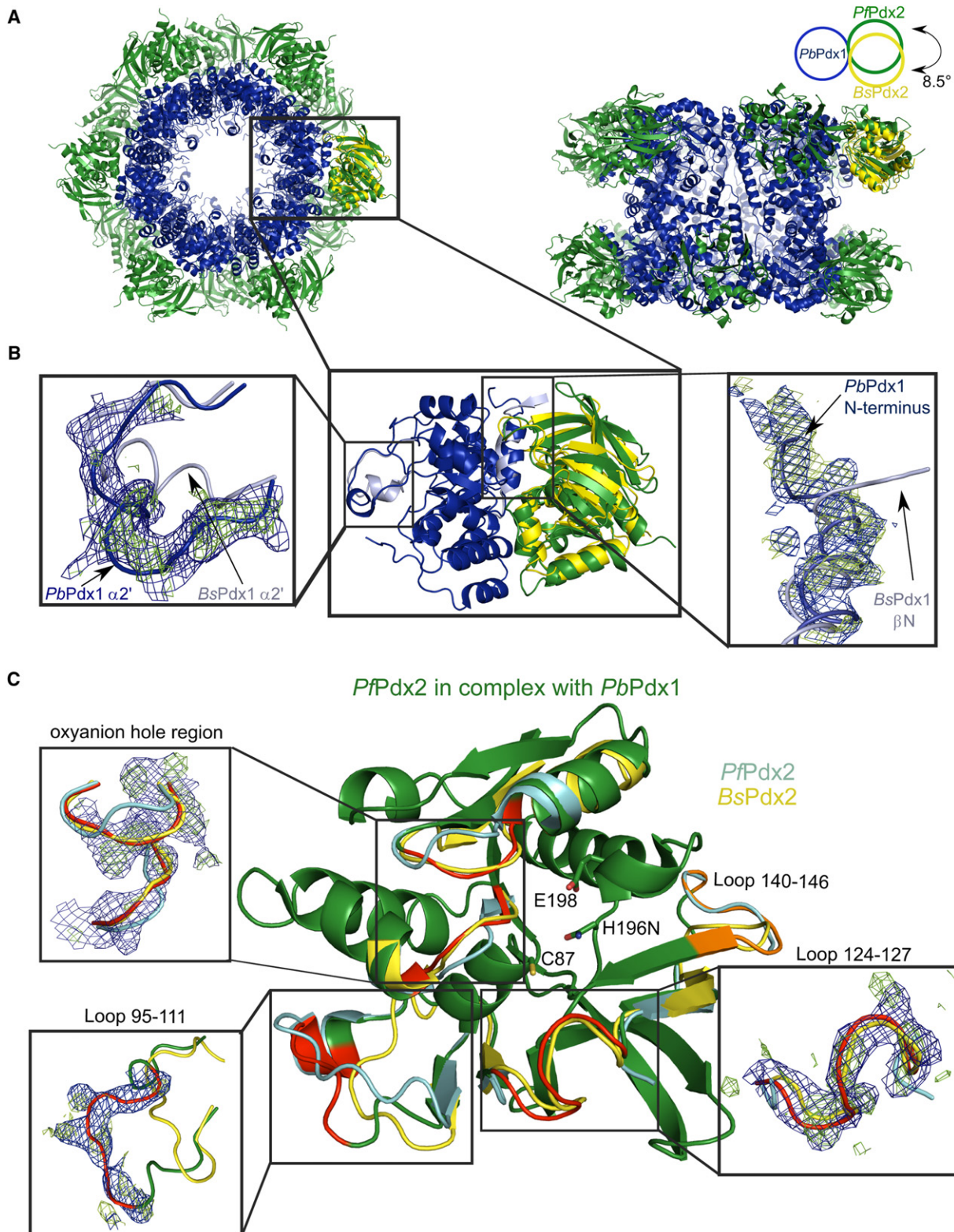
Figure 3. The Structure of the *Plasmodium* PLP Synthase Complex

(A) The PLP synthase/L-glutamine complex structure in two views, 90° rotated around an axis horizontal in the paper plane. The *Pb* Pdx1 dodecamer is shown in blue; the *Pf* Pdx2 subunits are shown in green. Superposition of plasmodial and bacterial (Strohmeier et al., 2006) PLP synthases, based on Pdx1, reveals different relative positioning of plasmodial and bacterial Pdx2 subunits (shown in yellow), as visualized in the schematic representation: the rotation by 8.5° is associated with a shift of 1.5 Å.

*Pb*Pdx2), compared with *Bs*Pdx2 (Gengenbacher et al., 2006). This region, labeled loop 95-111, is shown red in Figure 3C, and forms helix α5-1 at the interface to the α2-β3 loop in *Pf*Pdx1 (compare alignment in Figure S2A). The segment and, thus, the interaction are absent in bacterial complexes (Strohmeier et al., 2006; Zein et al., 2006). We conclude that the insertion sequences in plasmodial proteins, the differences in the N-terminal region of *Pb*Pdx1, and the different structure of the loop regions together explain the divergent thermodynamic signatures for complex formation between Pdx1 and Pdx2 in plasmodial and bacterial proteins as detected by calorimetry (Flicker et al., 2007; Neuwirth et al., 2007).

The Mode of Reciprocal Enzyme Activation, Derived from a Substrate Complex

The interaction between Pdx1 and Pdx2 fine-tunes the activity of the Pdx2 glutaminase (Wallner et al., 2009), and the mechanism of glutaminase activation has been well known for some time (Burns et al., 2005; Gengenbacher et al., 2006; Raschle et al., 2005; Strohmeier et al., 2006). Reorganization of the Pdx2 catalytic center is a major event in enzyme activation (Wallner et al., 2009). The Pdx2 subunit in the plasmodial PLP synthase complex reveals changes in the oxyanion region. The experimental electron density fit much better with the Pdx2 structure, as seen in the *Bs*Pdx1/*Bs*Pdx2 complex (Strohmeier et al., 2006), than with the input model (Gengenbacher et al., 2006) (PDB code 2ABW) and, hence, was rebuilt. These similarities observed in the *Bs*Pdx2 catalytic center imply that the mechanism of Pdx2 activation is conserved, despite the aforementioned documented differences in bacterial and plasmodial Pdx1/Pdx2 interfaces (Flicker et al., 2007; Neuwirth et al., 2007).

An open question is how Pdx1 is activated by complex formation and how ammonia production and incorporation into the forming PLP molecule are coordinated. In the *Bs* structures, helix α2′ was observed in the vicinity of the active site in the heteromeric *Bs*Pdx1/*Bs*Pdx2 PLP synthase complex but was disordered in autonomous Pdx1, which led us to postulate that this helix may prime the enzyme for catalysis (Strohmeier et al., 2006). However, helix α2′ was ordered in the yeast Pdx1 structure in the absence of Pdx2 (Neuwirth et al., 2009; Zhang et al., 2010). In plasmodial PLP synthase we now observe a "ground state" in this important region, giving additional insight into Pdx1 activation. Helix α2′ does not cover the proposed active site and is leaving ample access to the catalytic center (Figure 4A). This differs from the previously observed closed conformation in PLP synthase complexes from *Bs* or *T. maritima* (Strohmeier et al., 2006; Zein et al., 2006).

We wanted to investigate the significance of this finding and determine structures of Pdx1 in the absence or presence of substrate R5P (Table 2). Cocrystallization with the carbohydrate yielded crystals of the *Pb*Pdx1-R5P substrate complex (*Pb*Pdx1-R5P) that diffracted to 2.4 Å. Interestingly, helix α2′ is in a different position from the chimeric PLP synthase complex (Figure 4), closer to what was observed for *Bs* or *T. maritima* PLP synthase complexes and consistent with the active state of the *Pb*Pdx1 enzyme.

The 3D structure of the adduct complex showed the carbohydrate R5P in covalent linkage to Lys84, forming a Schiff base (Figure 4B). The structure is of considerable interest, given the ongoing controversies regarding the catalytic mechanism of PLP formation (Burns et al., 2005; Hanes et al., 2008a, 2008b, 2008c; Moccand et al., 2011; Raschle et al., 2007; Zhang et al., 2010). In the previous 2.9 Å resolution structure of *T. maritima* Pdx1, substrate attachment of the ribose at C2 was suggested (Zein et al., 2006), which was later corrected by chemical analysis (Hanes et al., 2008b). Accordingly, the complex reported here at higher resolution now confirms attachment at C1 (Figure 4B). The residues Asp105 and Ser107 of the totally conserved DESE motif were in close proximity to the substrate but did not make polar contacts. These residues may be involved in Schiff base formation and removal of water from C1. The covalent intermediate was shielded from the environment by helix α2′ and made very few polar contacts with the enzyme. One such polar contact occurred between the 2-OH group of the substrate and the carboxylate of the Asp27 side chain, which is totally conserved among Pdx1 enzymes. Asp27 could, therefore, have a catalytic role in water elimination from the carbon backbone. Finally, there were polar interactions between the oxygen atoms of the substrate phosphate group with three glycines (Gly156, Gly 217, and G238) and the Ser239 hydroxyl group from helix α8′ (Figure 4B). Helix α8′ points toward the phosphate group with its N-terminal dipole.

Methionine Residues Involved in Ammonia Transfer Link Ammonia Production, Transfer, and PLP Biosynthesis

On the reaction path toward the forming PLP molecules, ammonia is incorporated into the R5P adduct to form a stable chromophoric intermediate (Hanes et al., 2008b; Raschle et al., 2007). The site of ammonia production by Pdx2 is about 22 Å away from the site of ammonia incorporation in Pdx1. A transient hydrophobic tunnel operated by shifting methionine residues was proposed for the passage of ammonia (Strohmeier et al., 2006). With the exception of Met46 and Met148, these methionine residues are not conserved between eukaryotic and bacterial orthologs (Figures 5A, 5B, and S2A).

Three amino acid exchanges give the plasmodial Pdx1 ammonia tunnel a character different from the *Bs* protein. First, Trp16 in *Pb*Pdx1 replaces *Bs*Met13 in helix αN. Variation at this position was analyzed in the *Arabidopsis* protein, where

(B) Zoom of the *Pb*Pdx1/*Pf*Pdx2 heterodimer (blue/green) with the superposed bacterial *Bs*Pdx2 subunit. The electron density maps after molecular replacement (blue, 2mFo-DFc at 1.2 σ; green, Fo-DFc at 2.2 σ) with the final *Pb*Pdx1 models (blue) against the structures of *Bs*Pdx1 (gray) show the region of the N terminus and of the α2′ helix.

(C) View of the interface region of the *Pf*Pdx2 protein as observed in the PLP synthase complex (green). Several loop regions (red and orange) were seen in different conformation from the autonomous *Pf*Pdx2 (turquoise, PDB code 2ABW) (Gengenbacher et al., 2006). For comparison, loop regions for *Bs*Pdx2 as observed in the PLP synthase complex are also shown (yellow, PDB code 2NV2) (Strohmeier et al., 2006). Electron density maps after molecular replacement are shown for the oxyanion hole region, as well as the loops 95-111 and 124-127. Loop 140-146 is observed in a different conformation, but not part of the interface (orange). The catalytic triad Cys87, His196 (exchanged with asparagine), and Glu198 are shown in stick representation.
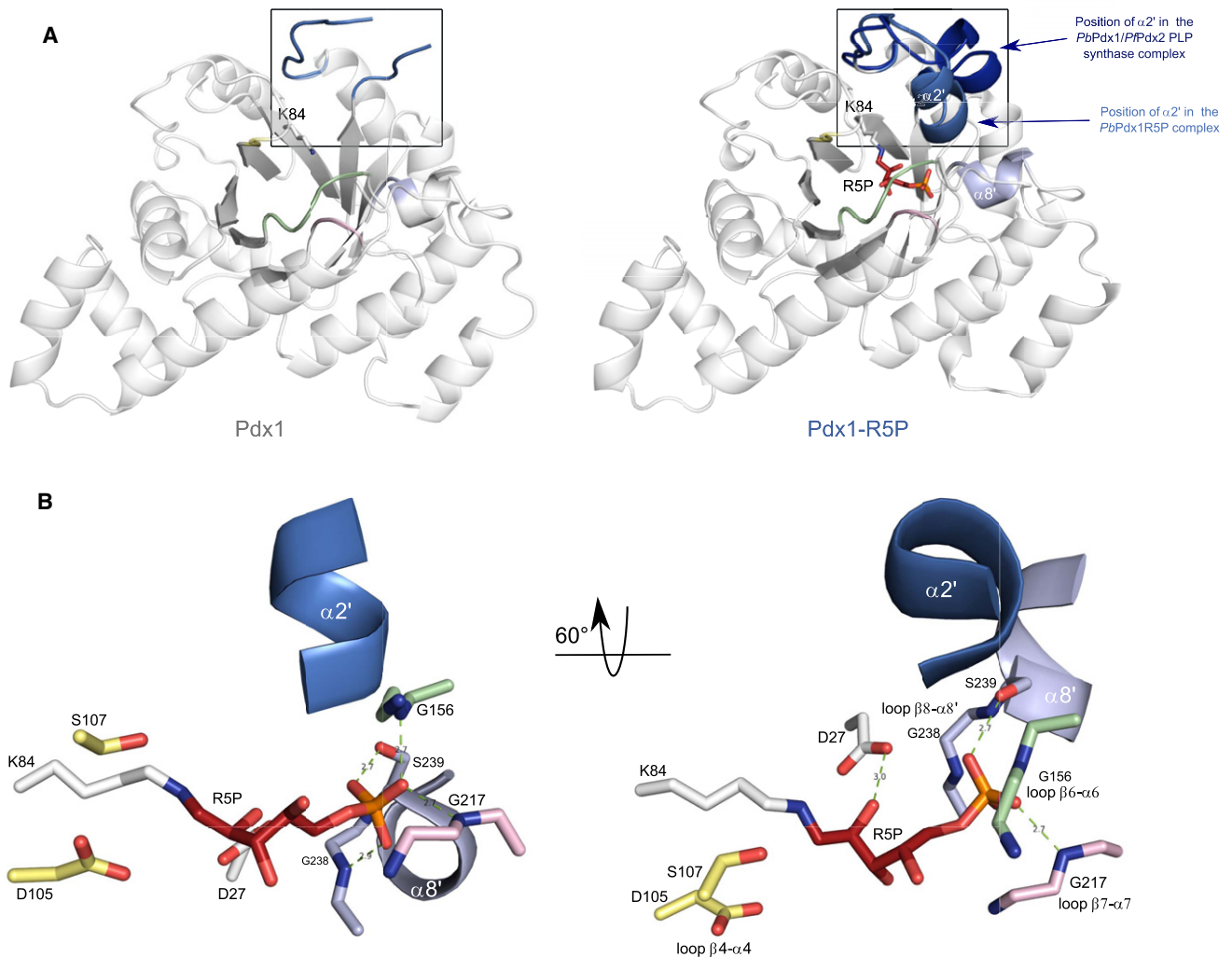
Figure 4. The *Pb*Pdx1-R5P Substrate Complex
(A) Comparison of Pdx1 monomers from autonomous *Pb*Pdx1 (left) and the *Pb*Pdx1-R5P substrate complex (right). The side chain of Lys84 and the covalent intermediate complex are shown in stick representation. Helix α2′ is observed in the closed conformation in the *Pb*Pdx1-R5P substrate complex, whereas it is in the open conformation in the *Pb*Pdx1/*Pf*Pdx2/L-glutamine PLP synthase complex (blue).
(B) Two views showing selected structural elements that define substrate binding, rotated by about 60° around a horizontal axis. The following protein-carbohydrate interactions are shown: the covalent R5P attachment between Lys84 and the C1 atom of R5P through a Schiff base; the contact between Asp27 and the C2-OH of R5P; backbone interactions with the R5P phosphate group (loop β6-α6, green; loop β7-α7, pink; loop β8-α8, light blue); and the contact between the hydroxyl group of Ser239 on α8′ with the R5P phosphate group. Residues Asp105 and Ser107 of the totally conserved DESE motif are seen in close proximity to the substrate and Lys84. Also shown are helices α2′ (blue) and α8′ (light blue) that change conformation upon substrate binding.

Leu30 is found in the equivalent position (Figure S2A). Our earlier mutagenesis study showed that this residue influences the coupling between Pdx2 glutaminase and Pdx1 synthase activities and possibly alters entrance into the tunnel (Tambasco-Studart et al., 2007). Interestingly, the exchange of *Pb*Trp16 for *Bs*Met13 is matched by a reciprocal exchange of *Pb*Met103 for *Bs*Tyr100. Finally, *Pb*Leu82 replaces *Bs*Met79. These three exchanges lead to differences in the construction of the putative ammonia tunnel, as seen from the position of cavities (Figure 5C). The reciprocal exchanges suggest a functional swap in methionines and flexibility in the construction of the tunnel.

We sought to confirm the role of methionine residues by site-directed mutagenesis and determination of associated enzy-

matic activities and determine Pdx2 glutaminase activity as well as PLP synthase activity both with ammonium salts or Pdx2 as source for the required ammonia. We also calculated the efficiency of enzymatic coupling as the ratio between Pdx2-dependent and ammonium salt-dependent PLP synthesis rates. Using this calculation, wild-type proteins show a ratio of 1.6. This indicates that the presence of Pdx2 has a stimulating effect on Pdx1 activity (Figure 6).

Replacement of *Pb*Met19 located in helix αN with valine halved the glutaminase activity but did not significantly affect PLP synthesis rates in the Pdx2-dependent assay, suggesting that this residue plays a role in glutaminase activation. In the ammonia-dependent assay we observed a doubling of PLP
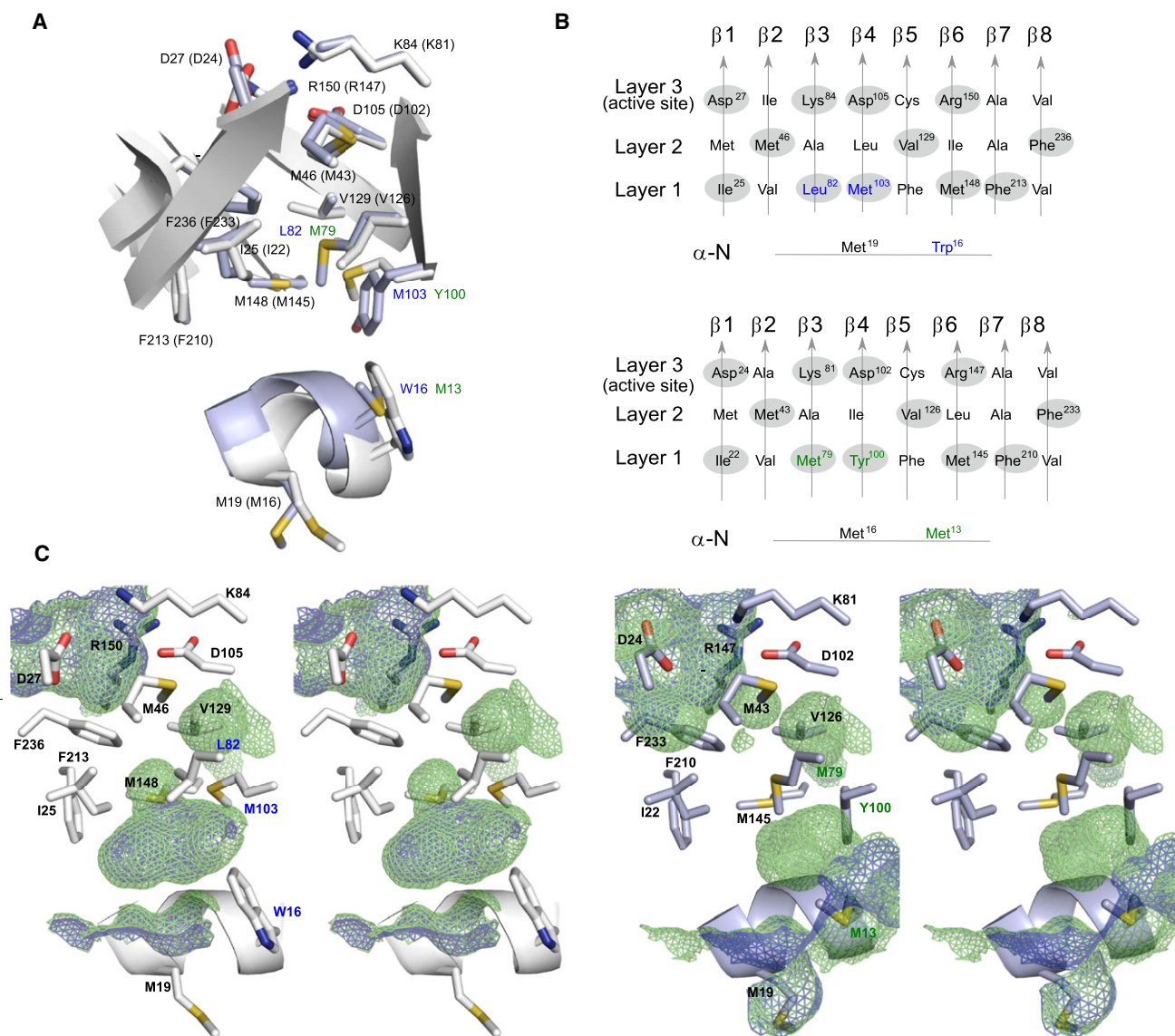
Figure 5. Ammonia Tunnel in *Pb* Pdx1

(A) View of the *Pb*Pdx1 β_8 barrel ($\beta2$ and $\beta3$ removed for clarity) and part of the αN helix. Selected side chains are shown in stick representation and labeled (gray), and residues from a superposed *Bs*Pdx1 are shown for comparison (light blue, labels in brackets, PDB code 2NV2) (Strohmeier et al., 2006).

(B) Schematic organization of the NH$_3$ tunnel with a comparison of *Pb*Pdx1 (top) and *Bs*Pdx1 (bottom). Residues pointing into the β_8 barrel are highlighted in gray. Differences discussed are marked in blue (*Pb*Pdx1) and green lettering (*Bs*Pdx1).

(C) Cavities in the NH$_3$ tunnel for *Pb*Pdx1 (left) and *Bs*Pdx1 (right), produced with a 1.2 Å (blue) and 1.4 Å (green) probe radius in PyMOL (DeLano, 2002).

synthase activities, and thus, exchange of this methionine with the smaller valine may have released a block at the tunnel entrance.

We grouped residues lining the tunnel through the central core of the β barrel in three layers. Layer 1 contains *Pb*Leu82, *Pb*Met103, and *Pb*Met148. Although variation of *Pb*Leu82 adversely affected PLP synthase activity in the ammonium salt-dependent assay, *Pb*Met103 lowered PLP synthase activities in both the ammonium salt and Pdx2-dependent assays. Complete loss of activity in the *Pb*Met103Phe variant suggested that the tunnel was impassable for ammonia. Even replacement of *Pb*Met103 with alanine showed lowered PLP synthase

activity, suggesting that Met103 is required for regulation of ammonia transfer. The most significant changes are observed in variation of Leu82 and Met148. Exchange of these residues resulted in approximately 4- to 5-fold higher ratios between Pdx2-dependent and ammonium salt-dependent PLP synthesis rates. These residues, therefore, directly link glutamine hydrolysis, ammonia transfer, and PLP production. This is in contrast to variation of the conserved *Pb*Met46 in layer 2, which leads to significant increase in PLP synthase activity in both types of assays, suggesting that this residue influences the function of the ammonia tunnel but does not function in enzyme communication.
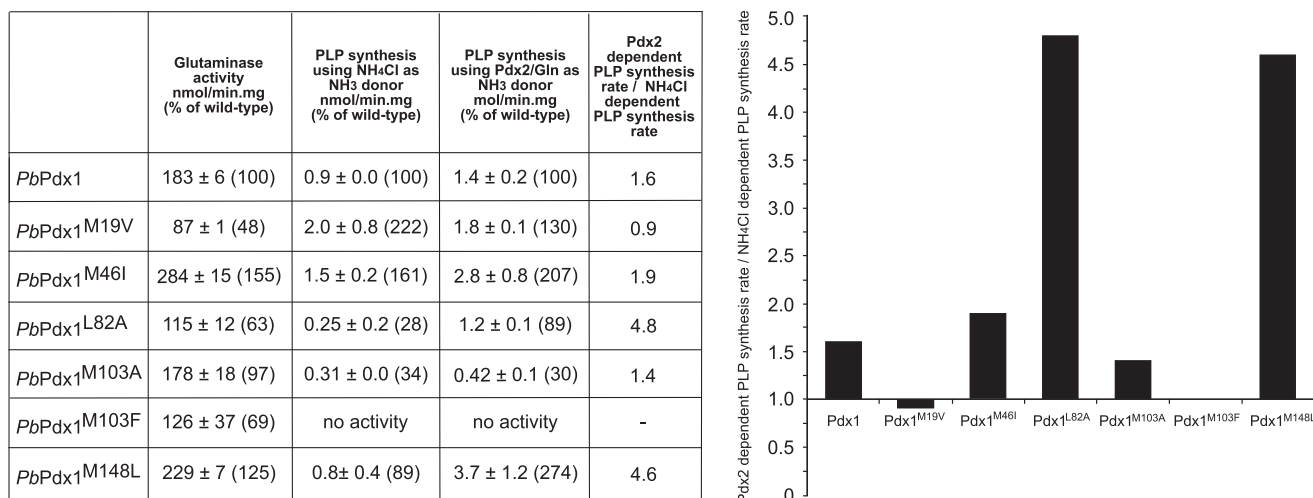
	Glutaminase activity nmol/min.mg (% of wild-type)	PLP synthesis using NH₄Cl as NH₃ donor nmol/min.mg (% of wild-type)	PLP synthesis using Pdx2/Gln as NH₃ donor mol/min.mg (% of wild-type)	Pdx2 dependent PLP synthesis rate / NH₄Cl dependent PLP synthesis rate
*Pb*Pdx1	183 ± 6 (100)	0.9 ± 0.0 (100)	1.4 ± 0.2 (100)	1.6
*Pb*Pdx1^M19V	87 ± 1 (48)	2.0 ± 0.8 (222)	1.8 ± 0.1 (130)	0.9
*Pb*Pdx1^M46I	284 ± 15 (155)	1.5 ± 0.2 (161)	2.8 ± 0.8 (207)	1.9
*Pb*Pdx1^L82A	115 ± 12 (63)	0.25 ± 0.2 (28)	1.2 ± 0.1 (89)	4.8
*Pb*Pdx1^M103A	178 ± 18 (97)	0.31 ± 0.0 (34)	0.42 ± 0.1 (30)	1.4
*Pb*Pdx1^M103F	126 ± 37 (69)	no activity	no activity	-
*Pb*Pdx1^M148L	229 ± 7 (125)	0.8± 0.4 (89)	3.7 ± 1.2 (274)	4.6

Figure 6. Mutagenesis and Kinetic Analysis of Pdx1 Variants

The columns in the table show the *Pb*Pdx2 glutaminase activity in the presence of *Pb*Pdx1 proteins and variants, as well as the PLP synthase activities of *Pb*Pdx1 proteins and variants in the presence of *Pb*Pdx2 or in the absence of *Pb*Pdx2 with ammonium salt as ammonium donor. The effect of Pdx2 was calculated as ratio of glutamine-dependent and -independent assay-specific activities and is plotted in the bar diagram. Values are the mean of two independent measurements.

DISCUSSION

PLP biosynthesis has received renewed interest since the discovery of the new route catalyzed by the Pdx1 and Pdx2 enzymes (Ehrenshaft et al., 1999; Mittenhuber, 2001). Several mechanistic studies on PLP biosynthesis by the enzymes Pdx1 and Pdx2 have recently appeared (reviewed in Fitzpatrick et al., 2007, 2010; Mukherjee et al., 2011). Structural descriptions were so far focused on prokaryotic systems (Strohmeier et al., 2006; Zein et al., 2006), and insight into orthologous eukaryotic PLP synthases is sparse (Neuwirth et al., 2009; Zhang et al., 2010). Further structural knowledge is required to understand documented differences between prokaryotic and eukaryotic systems in their biochemistry and in the interaction between Pdx1 and Pdx2 proteins (Flicker et al., 2007; Neuwirth et al., 2007). The potential impact as a drug target (Müller et al., 2010; Müller and Kappes, 2007) further provided a strong motivation to characterize the malarial enzymes.

Pf PLP synthase proved a difficult target for crystallographic 3D structure determination due to the observed aggregation into fibers in vitro, as detected by EM analysis. In contrast, fiber formation was not seen with the *Pb* proteins, and it will require further data to establish whether this finding can be generalized to other Pdx1 orthologs. We have compared the surfaces of the proteins to study the cause of fiber formation, but a mechanism was difficult to assign. An insertion in the *Pf*Pdx2 sequence (residues 95–111), varying between *Pf* and *Pb* proteins and not present in prokaryotic sequences, could mediate contacts in fibers. Because the chimeric complex contains *Pf*Pdx2, elements in the highly conserved Pdx1 protein must contribute to fiber formation. Indeed, the EM analysis not only detected fiber formation preferentially of the *Pf*Pdx1/*Pf*Pdx2 complex but also of the *Pf*Pdx1 proteins (data not shown). Circumstantial evidence comes from gel filtration analysis that shows that *Pf*Pdx1 proteins form higher-order oligomers after prolonged storage at 4°C,

whereas this is also true for the *Pf*Pdx1/*Pf*Pdx2 PLP synthase complex, albeit at a higher proportion (Figure S1).

Our previous study on *Plasmodium* Pdx1 demonstrated that hexamers are required for formation of the covalent enzyme-substrate adduct (shown in Figure 4) (Derrer et al., 2010). The C terminus of the protein responsible for hexamer formation probably has a function in *trans*, influencing the catalytic activity in a neighboring subunit in the hexameric form of Pdx1. To our knowledge, no data are currently available to give a molecular rationale for dodecamer formation. Indeed, the yeast Pdx1.1 protein is hexameric with equal or higher catalytic activity than dodecameric Pdx1 homologs (Neuwirth et al., 2009). Although an even higher organization into fibers shown here may not be catalytically relevant, fibers may provide a storage pool, perhaps protecting the viable C terminus that is prone to degradation (Raschle et al., 2009). A similar behavior of higher-order oligomerization has been seen in the AAA-ATPase Vps4p (Hartmann et al., 2008). It is an open question whether fibers could be identified at physiological conditions; however; fiber formation may be relevant to explain our previous data that revealed an uneven distribution of the two proteins within the cytosol in blood stages of the parasite (Gengenbacher et al., 2006). *Pf*Pdx1 shows a punctuate pattern in immunofluorescence analysis, indicating that there might be a higher-ordered structure; whether this is due to fiber formation or reflects a different level of structural organization will require further investigation. PLP biosynthesis is rather ineffective, and the specific activity of the *Pf*Pdx1/*Pf*Pdx2 complex was determined to be 662 ± 54 pmol min⁻¹ mg⁻¹ (Müller et al., 2008). Its activity may well be regulated by interacting proteins that may be activators of PLP biosynthesis or sequester the enzymatic cofactor PLP, either directly or via chaperones. Assembly or disassembly of fibers could modulate these activities. Thus, the fibers observed present an exciting new opportunity to investigate Pdx1 regulatory circuits.

Autonomous *Pb*Pdx1 was dodecameric, as is characteristic for prokaryotic Pdx1 proteins (Strohmeier et al., 2006; Zein et al., 2006; Zhu et al., 2005). This observation emphasizes the difference with the Pdx1 protein from *S. cerevisiae* that was hexameric in the crystal structure and almost exclusively hexameric in solution (Neuwirth et al., 2009). In the yeast protein a unique sequence variation not present in *Pb*Pdx1 was responsible for the different oligomerization behavior (Neuwirth et al., 2009). The *Plasmodium* structure confirms that eukaryotic Pdx1 proteins, in general, can assemble into dodecameric structures.

From the EM studies we gained new insights into PLP protein complex assembly. The *Pb*Pdx1 dodecamers were randomly occupied by *Pb*Pdx2 subunits, and none of the electron microscopic data showed any preference for the *Pb*Pdx2 association, and in particular there seemed to be no requirement for neighboring or alternating binding sites to be occupied. We tested against the presence of Pdx1 substrate R5P but did not detect differences in complex formation. Fully occupied complexes require the presence of glutamine and inactivation of the Pdx2 subunit by exchange of catalytic residues (Strohmeier et al., 2006). Under these conditions the encounter complex between Pdx1 and Pdx2 is converted to the more stable Michaelis complex (Flicker et al., 2007; Neuwirth et al., 2007). The electron microscopic data presented here now suggest that after glutamine hydrolysis, Pdx2 not only reverts to the encounter complex but also leaves the complex. Alternatively, encounter complexes must have high off rates.

Aggregation of *Pf* PLP synthase samples into fibers, whereas in itself an interesting result, prohibited crystallization. We resorted to crystallize a chimeric complex between *Pb*Pdx1 and *Pf*Pdx2. The reconstituted PLP synthase was fully functional with respect to glutaminase and PLP synthase activities, suggesting that the *Pb*Pdx1 and *Pf*Pdx2 proteins interact in a way that allows for enzyme activation. Availability of this enzymatically fully active complex enabled not only crystallization of a *Plasmodium* PLP synthase but also the 3D structure determination at resolution higher than that possible with the *Pb* PLP synthase complex. The approach to address relevant biological questions by combining proteins from different species in multiprotein complexes has proven to be a valuable approach in crystallography in general and may, with the *Plasmodium* proteins in particular, help to circumvent some of the pertinent problems in protein production (Mehlin, 2005; Mehlin et al., 2006).

Structure determination of PLP synthase by molecular replacement and subsequent NCS refinement at 3.6 Å benefitted from availability of high-resolution models (2.4 Å for *Pb*Pdx1, this study, and 1.6 Å for *Pf*Pdx2, PDB entry 2ABW). The resulting electron density map visualized structural differences from the input models, in well-ordered regions even for side chains. Structural differences mainly occurred at protein interfaces and explain the differences in the interaction of prokaryotic and eukaryotic PLP synthases, as described earlier (Flicker et al., 2007; Neuwirth et al., 2007). Eukaryotic structures differ from their prokaryotic counterparts by sequence insertion in Pdx2, which in *Pf*Pdx2 is found in the loop comprising amino acids 95–111 (Gengenbacher et al., 2006), and a smaller insertion can also be identified in the *Arabidopsis thaliana* Pdx2 sequence (Figure S2B). This loop is observed in different positions in the

structures of autonomous *Pf* Pdx2 and the *Pb*Pdx1/*Pf*Pdx2 PLP synthase complex. Furthermore, the loop connecting β6 and β7 is disordered in autonomous Pdx2 but ordered in the PLP synthase complex where it is part of the Pdx1-Pdx2 interface. The segment N terminal to helix αN in *Pb*Pdx1 does not interact with *Pf*Pdx2, in contrast to previous bacterial structures. This explains why we could not detect differences in the interaction of *Pf*Pdx1 and *Pf*Pdx2 when deleting this segment (Flicker et al., 2007). The latter abates the general importance of β augmentation for plasmodial PLP synthase.

Pdx1 is cooperative (Raschle et al., 2009) and relies on the C-terminal region for catalysis. The entire C terminus is required for full PLP synthase activity (Derrer et al., 2010), and a large part of the C terminus is resolved here, missing only the 14 most C-terminal residues. The resolved protein region is sufficient for PLP synthesis, as demonstrated in our previous C-terminal deletion studies in *Pf* Pdx1 (Derrer et al., 2010). The resolved C terminus contacts the loop between β6 and α6 of the same subunit and is in close proximity to helix α2′ of an adjacent subunit. Importantly, we show here two different structures for the α2′ region, depending on either formation of the PLP synthase complex or substrate binding (Figure 4A). The cooperative mechanism of PLP biosynthesis might thus rely on the active role of the C terminus in moving the helix α2′ that subsequently covers the active site and sequesters the reaction intermediates from the aqueous environment. Conversion from the open to the closed state of helix α2′ is not dependent on Pdx2 because Pdx1 alone forms covalent R5P intermediates. However, Pdx2 promotes an ordering of helix α2′, explaining why contact between Pdx1 and Pdx2 enhances R5P binding (Raschle et al., 2009). These findings give structural evidence how Pdx2 actively influences the catalytic state of the Pdx1 synthase.

Finally, the structures of the autonomous *Pb*Pdx1 and covalent enzyme substrate complex allow three important advances in the understanding of PLP synthase: (1) the alternative positioning of helix α2′, suggesting a regulatory layer in PLP synthase activation; (2) the assignment of the pentose substrate in Schiff base with the catalytic Lys84 attached on the ribose C1 atom; and finally, (3) the role of the β barrel in NH$_3$ transfer. Remarkably, the plasmodial proteins reveal plasticity in the construction of the ammonia tunnel. The features of ammonia transfer and catalytic mechanism allow us to understand—arguably—one of the most complex enzymatic systems known to date, and several of these unique features are exploitable in drug design.

EXPERIMENTAL PROCEDURES

Chemicals

3-acetylpyrimidine adenine dinucleotide (APAD), L-glutamic dehydrogenase from bovine liver, L-glutamine, DL-G3P, and R5P were from Sigma-Aldrich, Vienna. Imidazole was from Merck Darmstadt, Germany. KCl, NaH$_2$PO$_4$, and EDTA were from AppliChem GmbH, Darmstadt, Germany. NaCl was from AnalaR Normapur, Belgium. All other chemicals and reagents were from Roth, Karlsruhe, Germany.

Molecular Biology, Protein Production, and Purification

The *pdx1* gene was amplified from cDNA of the *Pb* NK65 strain using custom primers (Invitrogen Karlsruhe, Germany) and subsequently cloned into pET21a expression vector (Novagen, USA), using NdeI and XhoI restriction sites (enzymes from New England BioLabs, Frankfurt). The *pdx1* and *pdx2* genes

from *Pf* 3D7 strain and *pdx2* from *Pb* NK65 were cloned as described (Gengenbacher et al., 2006). *Pb*Pdx2 was subcloned into pET24a.

His-tagged *Pb*Pdx1 or *Pf*Pdx1 and *Pb*Pdx2 or *Pf*Pdx2 proteins were recombinantly expressed at 37°C in *Escherichia coli* BL21-CodonPlus (DE3)-RIL cells (Stratagene, USA). Cells were grown to an OD_{600} of 0.6, induced by addition of 0.1 mM isopropyl thiogalactoside, and then further grown for 4 hr. The cells were harvested by centrifugation and stored at −20°C. Proteins were purified by immobilized metal ion affinity chromatography using Ni-nitrilotriacetic-acid agarose beads (GE Healthcare Uppsala), equilibrated with lysis buffer (50 mM NaH_2PO_4 [pH 8.0], 300 mM NaCl, 10 mM imidazole). Protein-bead mixtures were washed with wash buffers (lysis buffer containing 10 mM imidazole and 50 mM imidazole, respectively) and eluted with elution buffer (lysis buffer containing 240 mM imidazole). For subsequent size exclusion chromatography of *Pb*Pdx1 or *Pf*Pdx1, a Superdex 200 26/60 column (GE Healthcare) equilibrated with 20 mM Tris/HCl (pH 8.0) buffer containing 10 mM NaCl, 1 mM EDTA, 0.5 mM mono-thioglycerol (MTG) was used. For *Pb*Pdx2 or *Pf*Pdx2 a Superdex 75 26/60 column (GE Healthcare) equilibrated with 20 mM HEPES (pH 7.0) buffer containing 300 mM KCl, 0.5 mM MTG was used. Fractions containing the desired protein were pooled and concentrated using Amicon Ultra filters (Millipore, Ireland).

Determination of Enzymatic Activities

The enzymatic activity for PLP synthesis was monitored spectrophotometrically at $\lambda = 414$ nm using a Jasco V550 Spectrophotometer (Jasco, Gross-Umstadt, Germany) according to the protocol described earlier (Raschle et al., 2005). Here, the purified proteins were exchanged into reaction buffer 50 mM Tris/HCl (pH 8.0), 20 mM NaCl using Amicon Ultra filters (Millipore). The reaction mixture contained 40 μM Pdx1, 1 mM R5P, 1 mM G3P, and 10 mM NH_4Cl. For Pdx1/Pdx2 complexes, additionally 40 μM Pdx2 was present, and NH_4Cl was replaced with 10 mM L-glutamine. Measurements were carried out at 37°C.

The enzymatic activity for glutamine hydrolysis was analyzed using a coupled enzyme assay with glutamate dehydrogenase as described earlier (Gengenbacher et al., 2006). The reaction mixture contained 5 μM Pdx1, 5 μM Pdx2, 10 mM L-glutamine, 10 U glutamate dehydrogenase, and 0.5 mM $APAD^+$ in 50 mM Tris/HCl (pH 8.0), 20 mM NaCl. The reduction of $APAD^+$ to APADH was monitored for 20 min at 30°C at 363 nm using a Jasco V550 Spectrophotometer.

Crystallography

*Pb*Pdx1 at a concentration of 20 mg/ml was crystallized by sitting or hanging drop vapor diffusion in 0.1 M bicine (pH 8.5) buffer containing 1.6 M LiCl buffer at 19°C. For the *Pb*Pdx1-R5P, crystallization was carried out in the presence of 10 mM R5P. The *Pb*Pdx1/*Pf*Pdx2^H196N/glutamine chimeric complex was prepared by mixing the two purified proteins at 1:1 stoichiometric ratio in a buffer containing 10 mM L-glutamine. The complex was crystallized at a concentration of 15 mg/ml in 0.1 M Na/K phosphate-phosphate buffer (pH 6.2) containing 0.2 M NaCl, 6% PEG 8000 by hanging drop vapor diffusion at 19°C. All crystals were flash frozen in liquid nitrogen, using additional 15% glycerol or 20% ethylenglycol in the crystallization buffer formulation, and stored under liquid nitrogen.

Data were collected at beamlines ID23-2 (*Pb*Pdx1), ID14-4 (*Pb*Pdx1-R5P), and ID23-1 (*Pb*Pdx1*Pf*Pdx2^H196N) at the European Synchrotron Radiation Facility (ESRF), Grenoble, France. Data were processed using *Denzo* and *Scalepack* (HKL Research). The *Pb*Pdx1 structure was solved by molecular replacement with *Bs*Pdx1 (Strohmeier et al., 2006) (PDB entry 2NV1) as a starting model, using Molrep (Collaborative Computational Project, Number 4, 1994). Iterative model building and refinement were carried out with Coot and Refmac5 (Collaborative Computational Project, Number 4, 1994). Water molecules were added to the model using ARP/wARP (Collaborative Computational Project, Number 4, 1994). The *Pb*Pdx1-R5P complex was determined by molecular replacement using Molrep (Collaborative Computational Project, Number 4, 1994) with *Pb*Pdx1 determined here and *Pf*Pdx2 determined earlier (Gengenbacher et al., 2006) (PDB entry 2ABW). The initial model was rigid body refined using Refmac5 (Collaborative Computational Project, Number 4, 1994) against data that were sharpened in B by 20 Å². The original models were rebuilt in very few loop regions (as described in the main text), followed by five cycles of atomic/TLS refinement with NCS applied to Pdx1 and to

Pdx2. We used NCS operators with tight restraints on main-chain atoms and loose restraints on side-chain atoms. All Pdx1 molecules were grouped together. Based on crystal contacts, Pdx2 chains G, I, and L and Pdx2 chains H, J, and K were refined in separate groups. The structure of the *Pb*Pdx1-R5P substrate complex was determined using molecular replacement with the *Pb*Pdx1 structure determined here. The ligand was built using the CCP4 library sketcher (Collaborative Computational Project, Number 4, 1994). Details of data processing and refinement statistics are given in Table 2.

Structure superposition of *Pb*Pdx1/*Pf*Pdx2^H196N with *Bs*Pdx1/*Bs*Pdx2^H170N was carried out using lsqkab (Collaborative Computational Project, Number 4, 1994). The rotation matrix obtained was used to calculate the rotation angle and translation of Pdx2 subunit. All structural diagrams were drawn using PyMOL (DeLano, 2002).

EM

Protein samples of *Pb*Pdx1 or *Pf*Pdx1 in complex with *Pb*Pdx2, *Pb*Pdx2^H199N, or *Pf*Pdx2^H196N in 50 mM Tris/HCl (pH 8.0) buffer containing 20 mM NaCl with or without 10 mM glutamine at a concentration of 20 μg/ml were stained with 2% uranyl acetate using the sandwich technique (Diepholz et al., 2008). Micrographs were recorded either with a CM120 Biotwin electron microscope at 100 kV and a nominal magnification of 52,000× on a 4kx4k Tietz-CCD-camera, or with a FEI F20 electron microscope at 200 kV with a nominal magnification of 29,000× on a Tietz 8kx8k CMOS camera. The pixel size was 2.36 Å/pixel for the CM120 and 2.69Å/pixel for the F20. For image analysis, particle images were semiautomatically selected with the autobox option of Boxer (Ludtke et al., 1999). Subsequent alignment and classification were done with IMAGIC 5 (van Heel et al., 1996).

ACCESSION NUMBERS

The PDB accession numbers for the structures reported in this paper are 4ads, 4adt, and 4adu.

SUPPLEMENTAL INFORMATION

Supplemental Information includes two figures can be found with this article online at doi:10.1016/j.str.2011.11.015.

REFERENCES

Burns, K.E., Xiang, Y., Kinsland, C.L., McLafferty, F.W., and Begley, T.P. (2005). Reconstitution and biochemical characterization of a new pyridoxal-5′-phosphate biosynthetic pathway. J. Am. Chem. Soc. *127*, 3682–3683.

Burrows, J.N., Chibale, K., and Wells, T.N. (2011). The state of the art in anti-malarial drug discovery and development. Curr. Top. Med. Chem. *11*, 1226–1254.

Bustamante, C., Batista, C.N., and Zalis, M. (2009). Molecular and biological aspects of antimalarial resistance in *Plasmodium falciparum* and *Plasmodium vivax*. Curr. Drug Targets *10*, 279–290.

Collaborative Computational Project, Number 4. (1994). The CCP4 suite: programs for protein crystallography. Acta Crystallogr. D Biol. Crystallogr. *50*, 760–763.

DeLano, W.L. (2002). The PyMOL Molecular Graphics System (San Carlos, CA: DeLano Scientific).

Derrer, B., Windeisen, V., Guédez Rodríguez, G., Seidler, J., Gengenbacher, M., Lehmann, W.D., Rippe, K., Sinning, I., Tews, I., and Kappes, B. (2010). Defining the structural requirements for ribose 5-phosphate-binding and inter-subunit cross-talk of the malarial pyridoxal 5-phosphate synthase. FEBS Lett. *584*, 4169–4174.

Dick, T., Manjunatha, U., Kappes, B., and Gengenbacher, M. (2010). Vitamin B6 biosynthesis is essential for survival and virulence of *Mycobacterium tuberculosis*. Mol. Microbiol. *78*, 980–988.

Diepholz, M., Venzke, D., Prinz, S., Batisse, C., Flörchinger, B., Rössle, M., Svergun, D.I., Böttcher, B., and Féthière, J. (2008). A different conformation for EGC stator subcomplex in solution and in the assembled yeast V-ATPase: possible implications for regulatory disassembly. Structure *16*, 1789–1798.

Divo, A.A., Geary, T.G., Davis, N.L., and Jensen, J.B. (1985). Nutritional requirements of *Plasmodium falciparum* in culture. I. Exogenously supplied dialyzable components necessary for continuous growth. J. Protozool. *32*, 59–64.

Ehrenshaft, M., Bilski, P., Li, M.Y., Chignell, C.F., and Daub, M.E. (1999). A highly conserved sequence is a novel gene involved in de novo vitamin B6 biosynthesis. Proc. Natl. Acad. Sci. USA *96*, 9374–9378.

Eliot, A.C., and Kirsch, J.F. (2004). Pyridoxal phosphate enzymes: mechanistic, structural, and evolutionary considerations. Annu. Rev. Biochem. *73*, 383–415.

Fitzpatrick, T.B., Amrhein, N., Kappes, B., Macheroux, P., Tews, I., and Raschle, T. (2007). Two independent routes of de novo vitamin B6 biosynthesis: not that different after all. Biochem. J. *407*, 1–13.

Fitzpatrick, T.B., Moccand, C., and Roux, C. (2010). Vitamin B6 biosynthesis: charting the mechanistic landscape. ChemBioChem *11*, 1185–1193.

Flicker, K., Neuwirth, M., Strohmeier, M., Kappes, B., Tews, I., and Macheroux, P. (2007). Structural and thermodynamic insights into the assembly of the heteromeric pyridoxal phosphate synthase from *Plasmodium falciparum*. J. Mol. Biol. *374*, 732–748.

Gengenbacher, M., Fitzpatrick, T.B., Raschle, T., Flicker, K., Sinning, I., Müller, S., Macheroux, P., Tews, I., and Kappes, B. (2006). Vitamin B6 biosynthesis by the malaria parasite *Plasmodium falciparum*: biochemical and structural insights. J. Biol. Chem. *281*, 3633–3641.

Hanes, J.W., Burns, K.E., Hilmey, D.G., Chatterjee, A., Dorrestein, P.C., and Begley, T.P. (2008a). Mechanistic studies on pyridoxal phosphate synthase: the reaction pathway leading to a chromophoric intermediate. J. Am. Chem. Soc. *130*, 3043–3052.

Hanes, J.W., Keresztes, I., and Begley, T.P. (2008b). 13C NMR snapshots of the complex reaction coordinate of pyridoxal phosphate synthase. Nat. Chem. Biol. *4*, 425–430.

Hanes, J.W., Keresztes, I., and Begley, T.P. (2008c). Trapping of a chromophoric intermediate in the Pdx1-catalyzed biosynthesis of pyridoxal 5′-phosphate. Angew. Chem. Int. Ed. Engl. *47*, 2102–2105.

Hansen, G., Heitmann, A., Witt, T., Li, H., Jiang, H., Shen, X., Heussler, V.T., Rennenberg, A., and Hilgenfeld, R. (2011). Structural basis for the regulation of cysteine-protease activity by a new class of protease inhibitors in Plasmodium. Structure *19*, 919–929.

Hartmann, C., Chami, M., Zachariae, U., de Groot, B.L., Engel, A., and Grütter, M.G. (2008). Vacuolar protein sorting: two different functional states of the AAA-ATPase Vps4p. J. Mol. Biol. *377*, 352–363.

Kappes, B., Tews, I., Binter, A., and Macheroux, P. (2011). PLP-dependent enzymes as potential drug targets for protozoan diseases. Biochim. Biophys. Acta *1814*, 1567–1576.

Knöckel, J., Müller, I.B., Bergmann, B., Walter, R.D., and Wrenger, C. (2007). The apicomplexan parasite *Toxoplasma gondii* generates pyridoxal phosphate de novo. Mol. Biochem. Parasitol. *152*, 108–111.

Knöckel, J., Jordanova, R., Müller, I.B., Wrenger, C., and Groves, M.R. (2009). Mobility of the conserved glycine 155 is required for formation of the active plasmodial Pdx1 dodecamer. Biochim. Biophys. Acta *1790*, 347–350.

Lakshmanan, V., Rhee, K.Y., and Daily, J.P. (2011). Metabolomics and malaria biology. Mol. Biochem. Parasitol. *175*, 104–111.

Ludtke, S.J., Baldwin, P.R., and Chiu, W. (1999). EMAN: semiautomated software for high-resolution single-particle reconstructions. J. Struct. Biol. *128*, 82–97.

Mehlin, C. (2005). Structure-based drug discovery for *Plasmodium falciparum*. Comb. Chem. High Throughput Screen. *8*, 5–14.

Mehlin, C., Boni, E., Buckner, F.S., Engel, L., Feist, T., Gelb, M.H., Haji, L., Kim, D., Liu, C., Mueller, N., et al. (2006). Heterologous expression of proteins from *Plasmodium falciparum*: results from 1000 genes. Mol. Biochem. Parasitol. *148*, 144–160.

Mittenhuber, G. (2001). Phylogenetic analyses and comparative genomics of vitamin B6 (pyridoxine) and pyridoxal phosphate biosynthesis pathways. J. Mol. Microbiol. Biotechnol. *3*, 1–20.

Moccand, C., Kaufmann, M., and Fitzpatrick, T.B. (2011). It takes two to tango: defining an essential second active site in pyridoxal 5′-phosphate synthase. PLoS One *6*, e16042.

Mooney, S., and Hellmann, H. (2010). Vitamin B6: killing two birds with one stone? Phytochemistry *71*, 495–501.

Mukherjee, T., Hanes, J., Tews, I., Ealick, S.E., and Begley, T.P. (2011). Pyridoxal phosphate: biosynthesis and catabolism. Biochim. Biophys. Acta *1814*, 1585–1596.

Müller, I.B., Knöckel, J., Groves, M.R., Jordanova, R., Ealick, S.E., Walter, R.D., and Wrenger, C. (2008). The assembly of the plasmodial PLP synthase complex follows a defined course. PLoS One *3*, e1815.

Müller, S. (2004). Redox and antioxidant systems of the malaria parasite *Plasmodium falciparum*. Mol. Microbiol. *53*, 1291–1305.

Müller, S., and Kappes, B. (2007). Vitamin and cofactor biosynthesis pathways in Plasmodium and other apicomplexan parasites. Trends Parasitol. *23*, 112–121.

Müller, I.B., Hyde, J.E., and Wrenger, C. (2010). Vitamin B metabolism in *Plasmodium falciparum* as a source of drug targets. Trends Parasitol. *26*, 35–43.

Neuwirth, M., Flicker, K., Strohmeier, M., Tews, I., and Macheroux, P. (2007). Thermodynamic characterization of the protein-protein interaction in the heteromeric *Bacillus subtilis* pyridoxalphosphate synthase. Biochemistry *46*, 5131–5139.

Neuwirth, M., Strohmeier, M., Windeisen, V., Wallner, S., Deller, S., Rippe, K., Sinning, I., Macheroux, P., and Tews, I. (2009). X-ray crystal structure of *Saccharomyces cerevisiae* Pdx1 provides insights into the oligomeric nature of PLP synthases. FEBS Lett. *583*, 2179–2186.

Percudani, R., and Peracchi, A. (2003). A genomic overview of pyridoxal-phosphate-dependent enzymes. EMBO Rep. *4*, 850–854.

Petersen, I., Eastman, R., and Lanzer, M. (2011). Drug-resistant malaria: molecular mechanisms and implications for public health. FEBS Lett. *585*, 1551–1562.

Raschle, T., Amrhein, N., and Fitzpatrick, T.B. (2005). On the two components of pyridoxal 5′-phosphate synthase from *Bacillus subtilis*. J. Biol. Chem. *280*, 32291–32300.

Raschle, T., Arigoni, D., Brunisholz, R., Rechsteiner, H., Amrhein, N., and Fitzpatrick, T.B. (2007). Reaction mechanism of pyridoxal 5′-phosphate synthase. Detection of an enzyme-bound chromophoric intermediate. J. Biol. Chem. *282*, 6098–6105.

Raschle, T., Speziga, D., Kress, W., Moccand, C., Gehrig, P., Amrhein, N., Weber-Ban, E., and Fitzpatrick, T.B. (2009). Intersubunit cross-talk in pyridoxal 5′-phosphate synthase, coordinated by the C terminus of the synthase subunit. J. Biol. Chem. *284*, 7706–7718.

Strohmeier, M., Raschle, T., Mazurkiewicz, J., Rippe, K., Sinning, I., Fitzpatrick, T.B., and Tews, I. (2006). Structure of a bacterial pyridoxal 5′-phosphate synthase complex. Proc. Natl. Acad. Sci. USA *103*, 19284–19289.

Tambasco-Studart, M., Tews, I., Amrhein, N., and Fitzpatrick, T.B. (2007). Functional analysis of PDX2 from *Arabidopsis*, a glutaminase involved in vitamin B6 biosynthesis. Plant Physiol. *144*, 915–925.

Tanaka, K., Tazuya, K., Yamada, K., and Kumaoka, H. (2000). Biosynthesis of pyridoxine: origin of the nitrogen atom of pyridoxine in microorganisms. J. Nutr. Sci. Vitaminol. (Tokyo) *46*, 55–57.

Tazuya, K., Adachi, Y., Masuda, K., Yamada, K., and Kumaoka, H. (1995). Origin of the nitrogen atom of pyridoxine in *Saccharomyces cerevisiae*. Biochim. Biophys. Acta *1244*, 113–116.

Tesmer, J.J., Sunahara, R.K., Gilman, A.G., and Sprang, S.R. (1997). Crystal structure of the catalytic domains of adenylyl cyclase in a complex with Gsalpha.GTPgammaS. Science *278*, 1907–1916.

Travassos, M.A., and Laufer, M.K. (2009). Resistance to antimalarial drugs: molecular, pharmacologic, and clinical considerations. Pediatr. Res. *65*, 64R–70R.

van Heel, M., Harauz, G., Orlova, E.V., Schmidt, R., and Schatz, M. (1996). A new generation of the IMAGIC image processing system. J. Struct. Biol. *116*, 17–24.

Wallner, S., Neuwirth, M., Flicker, K., Tews, I., and Macheroux, P. (2009). Dissection of contributions from invariant amino acids to complex formation and catalysis in the heteromeric pyridoxal 5-phosphate synthase complex from *Bacillus subtilis*. Biochemistry *48*, 1928–1935.

World Health Organization. (2010). Malaria. Fact Sheet *94*, 1.

Wrenger, C., Eschbach, M.L., Müller, I.B., Warnecke, D., and Walter, R.D. (2005). Analysis of the vitamin B6 biosynthesis pathway in the human malaria parasite *Plasmodium falciparum*. J. Biol. Chem. *280*, 5242–5248.

Wrenger, C., Knöckel, J., Walter, R.D., and Müller, I.B. (2008). Vitamin B1 and B6 in the malaria parasite: requisite or dispensable? Braz. J. Med. Biol. Res. *41*, 82–88.

Zalkin, H., and Smith, J.L. (1998). Enzymes utilizing glutamine as an amide donor. Adv. Enzymol. Relat. Areas Mol. Biol. *72*, 87–144.

Zein, F., Zhang, Y., Kang, Y.N., Burns, K., Begley, T.P., and Ealick, S.E. (2006). Structural insights into the mechanism of the PLP synthase holoenzyme from *Thermotoga maritima*. Biochemistry *45*, 14609–14620.

Zhang, X., Teng, Y.B., Liu, J.P., He, Y.X., Zhou, K., Chen, Y., and Zhou, C.Z. (2010). Structural insights into the catalytic mechanism of the yeast pyridoxal 5-phosphate synthase Snz1. Biochem. J. *432*, 445–450.

Zhu, J., Burgner, J.W., Harms, E., Belitsky, B.R., and Smith, J.L. (2005). A new arrangement of (beta/alpha)8 barrels in the synthase subunit of PLP synthase. J. Biol. Chem. *280*, 27914–27923.